An Active Wound Dressing for Controlled Convective Mass Transfer With the Wound Bed

Mario Cabodi,[1] Valerie L. Cross,[2] Zheng Qu,[1] Karen L. Havenstrite,[1] Suzanne Schwartz,[3] Abraham D. Stroock[1]

[1] School of Chemical and Biomolecular Engineering, Cornell University, Ithaca, New York 14853

[2] Department of Biomedical Engineering, Cornell University, Ithaca, New York 14853

[3] Department of Surgery, Weill Medical College of Cornell University, New York 10021

Received 15 June 2006; revised 18 August 2006; accepted 30 August 2006
Published online 14 November 2006 in Wiley InterScience (www.interscience.wiley.com). DOI: 10.1002/jbm.b.30723

Abstract: Conventional wound dressings—gauze, plastic films, foams, and gels—do not allow for spatial and temporal control of the soluble chemistry within the wound bed, and are thus limited to a passive role in wound healing. Here, we present an active wound dressing (AWD) designed to control convective mass transfer with the wound bed; this mass transfer provides a means to tailor and monitor the chemical state of a wound and, potentially, to aid the healing process. We form this AWD as a bilayer of porous poly(hydroxyethyl methacrylate) (pHEMA) and silicone; the pHEMA acts as the interface with the wound bed, and a layer of silicone provides a vapor barrier and a support for connecting to external reservoirs and pumps. We measure the convective permeability of the pHEMA sponge, and use this value to design a device with a spatially uniform flow profile. We quantify the global coefficient of mass transfer of the AWD on a dissolvable synthetic surface, and compare it to existing theories of mass transfer in porous media. We also operate the AWD on model wound beds made of calcium alginate gel to demonstrate extraction and delivery of low molecular weight solutes and a model protein. Using this system, we demonstrate both uniform mass transfer over the entire wound bed and patterned mass transfer in three spatially distinct regions. Finally, we discuss opportunities and challenges for the clinical application of this design of an AWD. © 2006 Wiley Periodicals, Inc. J Biomed Mater Res Part B: Appl Biomater 82B: 210–222, 2007

Keywords: wound dressings; wound healing; drug delivery; poly(hydroxyethyl methacrylate); poly(dimethylsiloxane)

INTRODUCTION

Acute cutaneous wounds and burns often involve damage to the underlying vascular structure; this damage can lead to impaired transport of metabolites and immunoresponsive factors to and from the wound site.[1–3] Chronic cutaneous wounds, such as those that develop in diabetic patients, suffer from an impaired healing response that is associated with biochemical imbalances, such as an excess of proteases, in the wound bed;[4,5] these wounds often fail to heal for weeks or months when treated with conventional wound dressings. Both of these classes of wounds would benefit from a tool that allows the clinician to monitor and control the soluble chemistry within the wound bed.

Conventional wound dressings—such as simple occlusive dressings—provide the basic functions required to allow wound healing, namely protection from outside agents and a barrier to evaporation. The advantages of conventional dressings are simplicity of application, familiarity, and low cost. The disadvantages of these dressings are the requirement of frequent changes, lack of specific biochemical or mechanical activity, and lack of external access to control and monitor the state of the wound bed.

Over the last three decades, biochemically and biologically functional dressings have been developed. These dressings include the dermal regeneration template Integra®,[6–8] and various biological dressings that incorporate living cells.[9,10] The advantages of these types of dressings are a tailored chemical environment that encourages the normal course of the healing process, extended periods between dressing changes, and the possibility of improved

Correspondence to: A. D. Stroock (ads10@cornell.edu)
Contract grant sponsor: Cornell Nanobiotechnology Center; contract grant number: ECS-9876771
Contract grant sponsors: Office of Naval Research Young Investigator Program, Cornell College of Engineering, Cornell University

clinical outcome relative to conventional dressings. The disadvantages are cost, complexity of application, and the fact that they do not provide any external access to monitor and control the state of the wound bed.

In the last decade, clinicians have been interested in the development of dressings that can be used to treat difficult wounds in both mechanically and chemically active ways; such active dressings could be used to inhibit infection by clearing pathogens and delivering antibiotics, to provide diagnostic information about the state of the wound in real-time, and to stimulate healthy healing responses. The vacuum-assisted closure (VAC®) therapy by Kinetic Concepts has become the most established mechanically active dressing. The VAC provides some of the above-mentioned capabilities, and over the past decade has become widely relied upon for the treatment of chronic wounds.[11–15] The VAC system consists of a soft, porous foam sponge made from poly(urethane) or poly(vinyl alcohol); the sponge is placed directly on the wound bed and covered with a plastic sheet. A vacuum is applied to the sheet via an embedded tube, and the foam dressing is compressed beneath the plastic. This action distributes mechanical stresses onto the tissue in the wound bed and mediates the perfusion of wound fluids through the tissue and into the evacuated exit. The mechanism of function of the VAC® in affecting healing is not well established, but it is hypothesized to be the result of a combination of mechanical stimulation of tissue activity (via deformation and fluid stresses)[15,16] and of regulation of the chemistry in the wound bed via perfusion with fluid. Recently, KCI has introduced a new system, the VAC® Instill®, that allows an external fluid to be perfused through the foam dressing; no analysis of this system has been reported in the literature to date.

Here, we present an active wound dressing (AWD) capable of delivery and extraction of solutes via externally controlled convective mass transfer (Figure 1). The device consists of two separate materials that we covalently bind to form a bilayer: a thin, porous sheet of poly(hydroxyethyl methacrylate) (pHEMA) that contacts the wound surface directly and carries a pressure driven flow, and a sheet of poly(dimethyl siloxane) (PDMS) that provides a vapor barrier and fluidic structures (fluid reservoirs and connections to the external pumping source). As illustrated schematically in Figure 1(B), the AWD can affect a wound in multiple ways: convective mass exchange from the surface of the wound bed, convective perfusion through the tissue, and application of mechanical stresses to the tissue. Our focus in the design and characterization of this dressing is on mass transfer—exchange of solute between the perfusing liquid and the wound bed. In a clinical context, the ability to generate well-defined mass exchange with the wound bed could be useful for the delivery of therapeutics, the elimination of destructive soluble factors in the wound, and the collection of chemical samples from the wound for diagnostic purposes. Furthermore, we show that our design allows active mass transfer with or without the application of significant mechanical stress on the wound bed; this decoupling mass exchange and mechanical action is not achievable with current AWDs, and may be useful clinically for the elucidation of the distinct roles of mass transfer and mechanical stimulation in defining the therapeutic function of active dressings. Potential weaknesses of our AWD for clinical application include the complexity of application and operation relative to conventional dressings and current active dressings, and binding of certain solutes to the dressings in a manner that complicates analysis of the exudates.

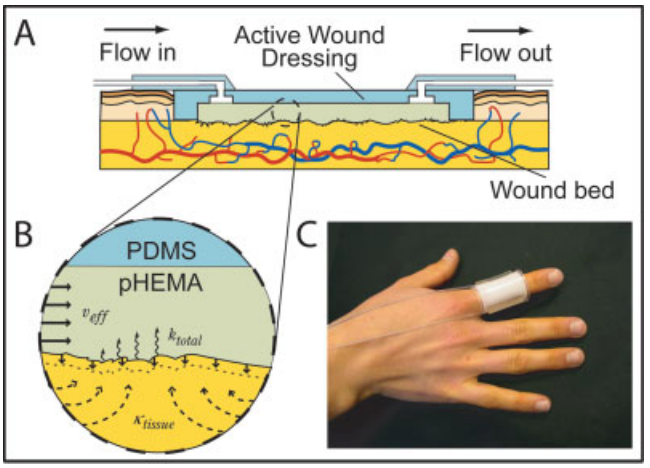

Figure 1. Active wound dressing. (A) Schematic cross-sectional view of an AWD placed in a wound bed, with input and output flow connections. (B) Expanded view of the interface between the AWD and the wound bed illustrating modes of action of AWD: the wiggly arrows represent convective mass transfer with mass transfer coefficient k_{total} (cm/s) into a flow through the porous pHEMA sponge; the dashed arrows represent flow through the tissue (which has hydraulic permeability κ_{tissue} (cm^2)); the bold arrows pointing into the tissue represent mechanical stress. (C) Image of an AWD adhered to a curved substrate (an uninjured index finger). [Color figure can be viewed in the online issue, which is available at www.interscience.wiley.com.]

The remainder of this paper is organized as follows: in the Materials and Methods section, we describe fabrication of the AWD and our experimental methods. In the Results section, we present characterization of materials used in the AWD and considerations for the design of the AWD. In the Discussion section, we begin with a quantitative characterization of the rate of mass exchange achieved with the AWD. We then present application of the AWD on a model wound bed made from calcium alginate gel. With this system, we demonstrate exchange of solutes (small molecules and proteins) mediated by the AWD, temporal analysis of the solutions extracted from the AWD, and spatially patterned mass exchange with a single substrate. In the Conclusion section, we finish with considerations for the application of the AWD in the clinic.

MATERIALS AND METHODS

Materials

2-Hydroxyethyl methacrylate (HEMA), ethylene glycol dimethacrylate (EGDMA), sodium chloride, *N*-vinyl pyrrolidone

(NVP), *N*,*N*,*N*′,*N*′-tetramethyl ethylene diamine (TEMED), ammonium persulfate (APS), dimethoxy phenyl acetophenone (DMAP), calcium chloride, *N*-(2-hydroxyethyl)-piperazine-*N*′-2-ethanesulfonic acid (HEPES), fluorescein disodium salt, fluorescein isothiocyanate labeled bovine serum albumin (FITC-BSA; MW = 67 kDa), and phenol red were purchased from Aldrich (St. Louis, MO) (www.sigma-aldrich.com). To remove unreacted fluorescein, the FITC-BSA was dialyzed in a dialysis cartridge (3500 MWCO; Slide-A-Lyzer, Pierce; 3–5 mL internal volume) against 3 L of HEPES buffer for 2 days. Alginate (LF10/60) was obtained from FMC Biopolymer (Philadelphia, PA) (www.fmcbiopolymer.com) as a powder and stored at −20°C until use. Methacryloxypropyl trimethoxysilane was purchased from Gelest (Morrisville, PA) (www.gelest.com). Tygon tubing (ID = 0.5 mm, OD = 1.0 mm), 16 gauge hypodermic needle, and Parafilm were purchased from Fisher Scientific (Hampton, NH).

Oxygen plasma treatments were performed in a plasma cleaner (model PDC-001, Harrick Scientific (Pleasantville, NY); www.harrricksci.com) on the highest power setting with an oxygen pressure between 300 and 350 mTorr. A high-intensity UV lamp (BIB-150P, Spectroline; 4.5 mW/cm^2 nominal intensity at bulb surface at 360 nm) was purchased from Fisher Scientific.

An airbrush (Badger 200NH, single-action air brush) was purchased from A.C. Moore (Ardmore, PA) (www.acmoore.com). Fluoresbrite® YG carboxylate microspheres (diameter = 0.1 μm) were purchased from Polysciences (Warrington, PA) (www.polysciences.com).

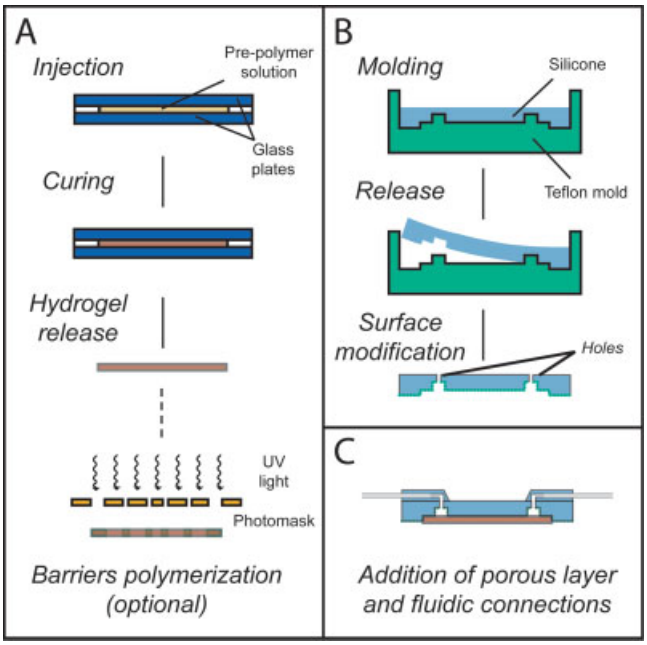

Figure 2. Fabrication process. (A) Synthesis of porous pHEMA. For the devices with multiple inlets, additional barriers were polymerized *in situ*, by soaking the pHEMA sheet in a solution containing photoinitiator and HEMA monomer, and exposing the sheet to UV light through a photomask. (B) Fabrication of silicone backing with reservoirs and connections for tubing. (C) Formation of complete AWD by covalently binding the pHEMA sheet and the PDMS layer to each other. PDMS tabs were attached on top of the reservoirs to connect the inlet and outlet tubing. [Color figure can be viewed in the online issue, which is available at www.interscience.wiley.com.]

Preparation of Porous pHEMA Hydrogel

A thin sheet of porous pHEMA was synthesized in a mold formed from two glass plates, as shown in Figure 2(A). The porosity was achieved by spontaneous phase separation of the pHEMA due to the presence of NaCl in the solution of monomer and cross-linker, as described by Liu et al.[17] A stock solution of monomer and cross-linker was formed as follows: HEMA monomer and ethylene glycol dimethacrylate (EGDMA) were mixed in a ratio of 99:1 (v/v); this solution was then mixed in a ratio of 1:2 (v/v) with a solution of 0.7*M* NaCl in deionized water.[17] A stock solution of 438 m*M* APS (0.1 g/mL, w/v) in deionized water was also prepared; this step facilitated the addition of the correct amount of APS to the solution to be polymerized (it was otherwise difficult to weigh out the small amounts of APS crystals required). Glass plates (10 × 10 cm^2) were washed, rinsed with ethanol, dried with a stream of nitrogen gas, and exposed to an oxygen plasma for 60 s to clean the surfaces. A mold for the polymerization of a pHEMA sheet was formed by clamping glass spacers (1.3-mm thick, cut from a standard glass slide) between the two glass plates and sealing the edge with Parafilm.

Just prior to injection in to the mold, 45 μL of TEMED (300 μ*M*) and 45 μL of the stock solution of APS (∼200 n*M*) were added to 10 mL of the solution of monomer and cross-linker and the combined solution was vortexed. The mixed solution was injected into the mold from a syringe with a hypodermic needle (16 gauge). Phase separation (signaled by an increase in opacity of the polymerizing mixture) was observed after ∼10 min. Polymerization was allowed to continue for a total of 120 min. This procedure resulted in pHEMA sheets that were flat, porous, and uniform over the entire 10 × 10 cm^2 area, as illustrated in Figure 3(A,B). The pHEMA sheets were intentionally created thicker than the corresponding recess in the PDMS layer [see Formation of PDMS Backing section and Figure 3(C)], such that the pHEMA layer was compressed beneath the silicone backing as the AWD was put under tension during operation.

To create a version of the AWD with three independent flow regions, additional barriers were photopolymerized into a layer of pHEMA formed as described in the proceeding paragraphs. This process proceeded as follows [Figure 2(C)]: After synthesis of the layer of pHEMA, excess water was extracted from the pHEMA sheet by compressing it lightly on a clean laboratory wipe. The sheet was then soaked with a solution of 1% (w/v) photoinitiator in neat HEMA monomer. The layer was then placed in contact with a photomask (comprising of three layers of printed transparencies glued together; 0.7 mm minimum feature size), clamped between two large glass slides, and exposed it to UV light

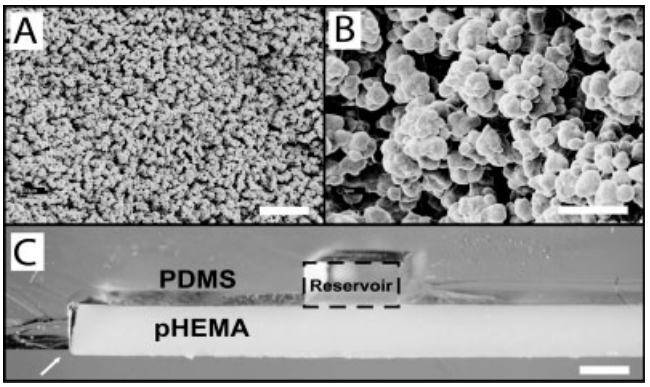

Figure 3. Microscopic structure of the pHEMA sponge. (A, B) Scanning electron micrographs of freeze-dried pHEMA. The scale bars are 50 and 10 μm for (A) and (B) respectively. (C) Optical image of cross-section of AWD, showing the PDMS layer with fluid reservoir, and the pHEMA sponge attached to it; the pHEMA layer is synthesized to be thicker than the recess in the PDMS layer (see arrow) to ensure that the sponge makes contact with the substrate after it is compressed by the applied vacuum (scale bar = 1 mm).

($\sim$4.5 mW/cm^2) for 5 min. The uncrosslinked solution was extracted by rinsing the pHEMA sheet in running water for 60 min. The resulting sheet with barriers was sealed to a functionalized PDMS layer as described in the following subsection.

Formation of PDMS Backing

Figure 2(B) illustrates the formation of the PDMS backing of the AWD by a molding process. A mold was formed in Teflon by mechanical machining. This mold contained topographical features to define a recessed area in the PDMS in which to lay the pHEMA layer, and fluid reservoirs to couple flow between external tubing and the pHEMA sheet (see Determination of Appropriate Dimensions of Inlet and Outlet Reservoirs section). The PDMS prepolymer was cast and cured on this mold for 2 h at 65°C. To allow for the formation of fluidic connections, holes were bored through the back side of the cured PDMS sheet to join the reservoirs. These holes were bored with a hypodermic needle (16 gauge), the tip of which had been cut flat and sharpened.[18] Connections to Tygon tubing were formed in one of two ways: in the first, the tubes were press-fit directly into the holes bored in the PDMS backing; this approach was simple, but required the PDMS backing to be at least 3-mm thick above the reservoirs in order to provide mechanical support to the tubing. In a second approach, tabs of PDMS with prebored holes were sealed to the backing by plasma activation of the surfaces[18] to act as supports of the tubing; this approach—shown schematically in Figure 2(B) and on the actual AWD in Figure 1(C)—was more complicated to implement but allowed the PDMS backing to be only 1-mm thick above the active region of the device. This second technique is required to achieve the flexibility demonstrated in Figure 1(C) and that would be necessary in clinical application.

Assembly of Wound Dressing

The silicone and pHEMA layers were formed independently prior to assembly, as described in the preceding two subsections. The sealing of these two layers to form the AWD proceeded as follows: a silanizing solution was prepared with 2% (v/v) methacryloxypropyl trimethoxysilane in 95% ethanol in water; the pH of this solution was adjusted to 5 using 0.1*M* HCl to favor hydrolysis of alkoxy groups to form silanol groups (adapted from Revzin et al.[19]). The PDMS layer was washed with ethanol, dried with nitrogen, and oxidized in oxygen plasma for 1 min; immediately after oxidation, this layer was immersed in a silanizing solution for 2 min, rinsed with ethanol, and allowed to sit at room temperature for $\sim$12 h (shorter delays after coating led to less reliable sealing to the pHEMA). The silanol groups reacted with the surface of the PDMS through a dehydration reaction, yielding a covalent bond between the PDMS and the coupling silane (Gelest). After this silanization step, a solution of photoinitiator and cross-linker (600 mg of dimethoxyphenyl acetophenone dissolved in 1 mL *N*-vinyl pyrrolidone and mixed with 1 mL EGDMA) was applied to the PDMS surface using an airbrush; the solution was sprayed until a uniform coating of the PDMS layer was obtained. We note that it is important that this solution be applied to the PDMS rather than to the pHEMA to ensure that the surface of the pHEMA is not obstructed by the film of EGDMA. The sheet of pHEMA was immediately placed in contact with the coated sheet of PDMS and exposed to UV light through the PDMS side for 10 min (intensity $\sim$4.5 mW/cm^2, obtained by placing the bilayers within 1 cm of the surface of the UV bulb); this exposure led to a uniform covalent seal between the two sheets. This bond was observed to persist for more than 12 months for bilayers stored in aqueous buffer; the seal was strong enough to withstand significant bending of the bilayer without delamination.

After the sealing step, the devices were rinsed in deionized water for 60 min, and stored in a buffered solution (HEPES buffered saline, pH 7.8). Before operation of the devices, Tygon tubing was press-fit into prebored holes in the PDMS.

Fabrication of Model Wound Beds

The wound dressing device was characterized on two types of substrates: a dissolvable block of benzoic acid and a nondissolvable calcium alginate hydrogel. The dissolvable substrate was used to measure the global mass transfer coefficient of the device (see Analysis of Mass Transport Mediated by Flow in a Porous Material section), while the nondissolvable substrate was used to demonstrate the spatial control of delivery/extraction of the device, and the effects of applied vacuum on soft, tissue-like substrates (see Operation of Advanced Wound Dressing section).

To create the dissolvable block, benzoic acid crystals were melted at a temperature of 250°C on a hot plate. The melt was poured into a stainless steel ring mold placed on

a polished silicon wafer. The melt was then cooled to room temperature and the stainless steel ring and silicon wafer were removed, yielding a disc 6 cm in diameter and 0.5 cm in thickness. The benzoic acid surface produced by contact with the silicon substrate was smooth and allowed for uniform contact with the AWD.

Calcium alginate substrates were prepared by steadily mixing 4 mL of a 5% (w/v) sodium alginate solution (36 m*M* sodium citrate) with 1 mL of a 2.5% (w/v) calcium sulfate solution for 30 s between two 10-mL syringes connected by a 3-way valve. The resulting mixture was injected between two glass plates separated by 1-mm thick spacers; this process is modified from Chang et al.[20] After 1 h, the plates were removed, and the alginate sheet was fully gelled by submersion in a solution of 60 m*M* calcium chloride in HEPES buffer for an additional hour. The gels were then stored in HEPES buffer supplemented with 10 m*M* $CaCl_2$, prior to use. The supplemental $CaCl_2$ in the buffer prevented dissolution of the calcium alginate gels that would occur by leaching of Ca^{2+} ions into a calcium-free bath.

Experimental Conditions

To drive fluid through the AWD, the inlet tubing was attached to a column of fluid the meniscus of which was maintained at the height of the wound bed, and the outlet tubing was attached to a peristaltic pump [Figure 4(A)]. Care was taken to ensure no air bubbles were introduced in the fluidic circuit. The device was placed on the substrate, and the peristaltic pump was operated to achieve flow rates ranging from 10^{-4} to 10^{-3} cm^3/s. At these flow rates, the pressure at the exit of the AWD was just below atmospheric pressure; this vacuum was sufficient to ensure adhesion of the dressing to the alginate substrate. Higher tensions were also achieved with an added resistance upstream of the AWD. Under these conditions, the liquid flowed continuously from the inlet reservoir to the peristaltic pump without formation of bubbles. For the benzoic acid discs, it was necessary to apply a thin layer of silicone grease to ensure sealing of the dressing to the rigid substrate; the grease was placed on the PDMS surface outside the footprint of the pHEMA sponge so as to avoid interference with the flow. We note that the role of the silicone grease is simply to prevent the vacuum-seal from being broken, since operation at subatmospheric pressures automatically provides the means to immobilize the device onto the substrate.

For the measurement of global mass transfer coefficient on benzoic acid substrates (see Analysis of Mass Transport Mediated by Flow in a Porous Material section), the devices were primed for ~1 h before collecting fractions for analysis. This priming step ensured that the fluid being analyzed had passed through the entire length of the AWD (steady-state extraction). Volumetric flow rates through the device were measured for all experiments by collecting the

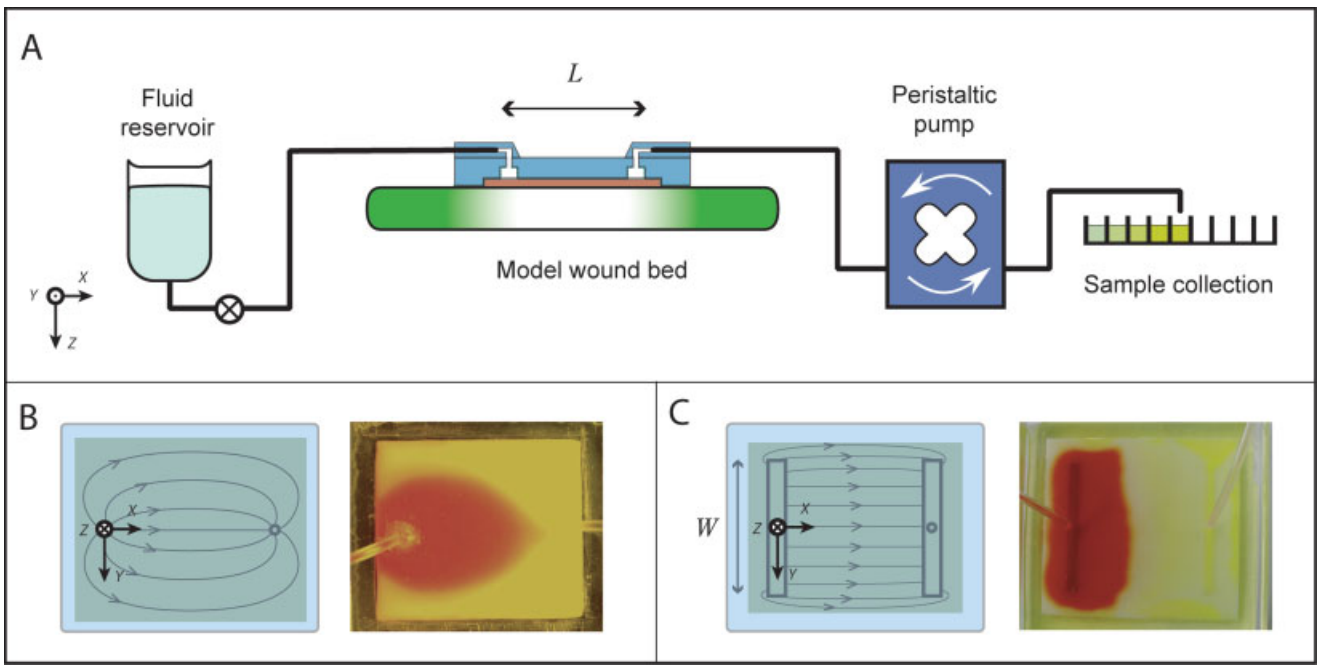

Figure 4. Design and operation of the AWD. (A) Experimental setup: the assembled device was placed on the substrate, a fluid reservoir was connected at the inlet with the meniscus maintained at the height of the substrate, and a peristaltic pump was connected at the outlet and the fluid exiting it was collected. (B) Expected streamlines (left) for small reservoirs devices and observed advancing front of a solution of dye driven between reservoirs formed by the bores of the Tygon tubing butted up against the pHEMA sponge. (C) Expected (left) and observed (right) advancing front of a solution of dye driven between extended, low resistance reservoirs. [Color figure can be viewed in the online issue, which is available at www.interscience.wiley.com.]

mass exiting the outlet on a balance over time. The concentration of dissolved benzoic acid collected from the outlet was determined with a UV–vis spectrophotometer (SpectraMax Plus 384, Molecular Devices). Absorbance readings were taken at 273 nm.

For the experiments on nondissolving substrate, sheets of alginate gel were soaked in a solution of 100 μM fluorescein or 50 μM FITC-BSA in HEPES buffer (for 1 h for fluorescein or 1 week for the FITC-BSA), prior to application of the AWD. For the extraction experiments (see Analysis of Exudate section), the wound dressing was placed on the dye-filled gels, and fractions of the exudate stream were collected into the wells of a 96-well plate every 4 min, as illustrated in Figure 4(A). A fluorescence plate reader (SpectraMax Gemini EM, Molecular Devices) was used for analysis of fluid collected from the device. A digital camera (Powershot G6, Canon) was used to acquire images of the device in operation and of the gels after operation.

RESULTS

Measurement of Hydraulic Permeability of pHEMA Sponge and Calcium Alginate Gel

We measured the hydraulic permeability of the porous pHEMA sponge and of the calcium alginate gels used as model wound beds. The specific permeability, κ_{pHEMA} (cm^2), was determined using a water column drip experiment, whereby the pressure drop and volume flow rate were measured. The volume flow rate, Q (cm^3/s), was measured gravimetrically on an analytical balance by collecting water that dripped through the sample (taking the density of water, $\rho = 1.0\ \mathrm{g/cm}^3$), while the pressure drop was determined by measuring the height of the column of fluid above the sponge surface. We calculated the permeability, κ (cm^2), using Darcy's law:[21]

$$Q = \frac{1}{R}\Delta P = \left(\frac{A\kappa}{\mu \Delta x}\right)\Delta P \qquad (1)$$

where Q (cm^3/s) is the volume flow rate, ΔP ($\mathrm{g/cm\ s}^2$) is the pressure difference, R ($\mathrm{g/s\ cm}^4$) is the hydraulic resistance to the flow, A (cm^2) is the cross-sectional area, μ (g/cm s) is the viscosity of the water, and Δx (cm) is the thickness of the porous material along the direction of the net flow.

Using the slope of the volume flow rate versus pressure drop curves, and the following values $\mu = 1 \times 10^{-2}$ g/cm s, $\Delta x = 0.1$ cm, and $A = 0.235\ \mathrm{cm}^2$, we calculated the hydraulic permeability of the pHEMA used in this work to be $\kappa_{\mathrm{pHEMA}} = 2.0 \times 10^{-9}\ \mathrm{cm}^2$. We used this value of the specific permeability in the Determination of Appropriate Dimensions of Inlet and Outlet Reservoirs section to aid design of the AWD, and in the Appendix to relate to the measured tortuosity, τ, of the porous pHEMA sponge. Using the same setup, we also measured the hydraulic permeability of the calcium alginate gels used in this work to be $\kappa_{\mathrm{alg}} = 3.0 \times 10^{-10}\ \mathrm{cm}^2$.

We used scanning electron micrographs such as those in Figure 3(A,B) to estimate the diameter of the pores in the pHEMA to be, $d_{\mathrm{pore}} \sim 10 \pm 4\ \mu\mathrm{m}$ (100 measurements in 10 images).

Determination of Appropriate Dimensions of Inlet and Outlet Reservoirs

Figure 4(A) presents a schematic diagram of the AWD mounted on a model wound bed. To generate a uniform flow within the porous layer (i.e., along the x-direction), the reservoirs must be designed appropriately. The use of small inlets and small outlets, such as those generated by simply butting the opening of Tygon tubing against the sponge, resulted in a "dipole-like" pressure field, with nonuniform flow within the sponge, as illustrated in Figure 4(B). This nonuniformity in the flow led to nonuniformity in the rate of mass transfer with the substrate (data not shown). To avoid this effect, we used low resistance fluid reservoirs at the inlets and outlets. The use of these reservoirs resulted in a uniform and uniaxial pressure gradient and flow along the x-direction within the porous material [Figure 4(C)].

The dimensions of the reservoir required for a uniform flow profile were determined as follows: the reservoirs should offer much less resistance to flow along their length, W (m) [see Figure 4(C)], than the fluid experiences as it flows from one reservoir to the other through the pHEMA sponge. If this condition is satisfied, constant pressure should be achieved along the boundaries of the sponge at $x = 0$ and $x = L$ under steady flow, and the flow between the reservoirs should be uniform (constant with respect to y) and uniaxial along x. This condition translates into a relationship between the hydraulic resistances of each reservoir and the pHEMA sponge: $R_{\mathrm{res}} \ll R_{\mathrm{pHEMA}}$, where R_{res} ($\mathrm{g/s\ cm}^4$) is the hydraulic resistance of the reservoir, and R_{pHEMA} is obtained from the hydraulic permeability of the sponge found earlier for Darcy flow in a porous material [see Measurement of Hydraulic Permeability of pHEMA Sponge and Calcium Alginate Gel section, Eq. (1)].

For flow along the reservoir, we take the resistance to be that of a laminar flow in a rectangular duct, such that:[22]

$$Q = \frac{1}{R_{\mathrm{res}}}\Delta P = \left(\frac{\pi d_{\mathrm{E}}^4}{128\mu(W/2)}\right)\Delta P \qquad (2)$$

where d_{E} is the equivalent diameter of the reservoir, W is the length of the reservoir, as in Figure 4(C), and Q, μ, and ΔP are defined above for Eq. (1). Using Eq. (2), and requiring that the resistance to flow in the reservoir be at least 10 times smaller than the resistance to flow inside the pHEMA sponge, we determined the minimum value for d_{E} to be 150 μm. We made fluid reservoirs of dimensions 1 mm in height and 2 mm in width, yielding an effective diameter of 1.5 mm, much larger than the minimum requirement. Figure 4(C) shows an advancing dye front in a dressing with this reservoir design; the minimal distortion of the front confirmed the validity of this approach.

Elution of Solutes though pHEMA Sponge

We observed that many of the solutes used in this study bind with the pHEMA sponge. We observed this phenomenon as a delay in the progression of the solute through the sponge when injected from the inlet in aqueous solution; the delay was relative to the movement of the solvent. This behavior is not entirely surprising, given that pHEMA beads are used as stationary phase in certain chromatographic applications.[23]

By looking at the theory of affinity chromatography, we can gain some insight into the effects of binding of solutes on the operation of AWD. Following Ravindranath,[24] the retention time, t_r (s), required for a binding solute to elute from a stationary phase (in this case the pHEMA sheet) is given by:

$$t_r = t_m(1 + \beta K_{s-m}) \quad (3)$$

In Eq. (3), t_m (s) is the elution time for the mobile phase (in this case, the buffer) and is defined by the volumetric flow rate, Q (cm^3/s) and the open volume within the porous medium, V_m (cm^3), such that $t_m = V_m/Q$, β ($=V_m/V_s$) is the ratio of the void volume, V_m, to the volume of the solid phase, V_s (i.e., the pHEMA), and $K_{s-m} = C_s/C_m$ is the distribution constant, defined as the ratio of concentration of the solute in the stationary phase, C_s (mol/L), to its concentration in the mobile phase, C_m (mol/L), at equilibrium. In our system, the retention time of a binding solute, t_r, can be thought of as a "retardation time" introduced by its interaction with the pHEMA, and will roughly correspond to the delay in detection of the solute in the collected exudate.

We checked whether each solute bound to the sponge by running it independently in the incoming stream, and comparing the observed elution time, t_r, with the residence time of the mobile phase, $t_m = V_m/Q$. Table I presents these values, as well as the distribution coefficient calculated with Eq. (3), with the phase ratio, $\beta = 0.5$. For example, we found that FITC-BSA eluted with no delay relative to the solvent ($t_r = t_m = 5$ min), such that $K_{pHEMA\text{-}buffer} = 0$. On the other hand, the elution time for fluorescein in water was, $t_r = 76$ min, relative to an elution time of the mobile phase ($t_m = 5$ min), such that $K_{pHEMA\text{-}buffer} \sim 28$ from Eq. (3). The data in Table I indicate that pHEMA has a substantial affinity for hydrophobic solutes. We discuss the implications of this binding on the operation of the AWD in the Analysis of Exudate section.

TABLE I. Affinity of Solutes for pHEMA

Solute	Distribution Coefficient (K)
BSA-FITC in buffer	0
Fluorescein in buffer	28
Fluorescein in water	∞ (never eluted)
Phenol red in buffer	34
Phenol red in water	18
Benzoic acid in water	0
Green food dye in water	28

The pH of the buffer was 7 and the pH of the water was 5.

DISCUSSION

Analysis of Mass Transport Mediated by Flow in a Porous Material

The AWD is a device for exchanging solutes with wounds. One quantitative measure of the efficiency of the AWD for this process is the global coefficient of interfacial mass transfer that it provides when placed in contact with a solid boundary. By solid boundary, we refer to one that is impermeable to convection (i.e., with specific Darcy permeability, κ_{tissue} much lower than that of the pHEMA sponge, $\kappa_{pHEMA} = 2.0 \times 10^{-9}$ cm^2—see Measurement of Hydraulic Permeability of pHEMA Sponge and Calcium Alginate Gel section), but that can exchange solute by diffusion. In this situation, the flow of fluid driven through the dressing will be confined to pHEMA sponge and will not pass through the underlying tissue. Such a boundary mimics a tissue of low Darcy permeability, such as ligament ($\kappa_{lig} \sim 10^{-15}$ cm^2)[25] or cartilage ($\kappa_{cart} \sim 10^{-14}$ cm^2).[26] We will use solid benzoic acid to mimic such a tissue.

To treat the limiting case of an impermeable substrate, we use the formalism of convective mass transfer in dilute solution, such that the global mass transfer coefficient, k_{AWD} (cm/s), is defined as:

$$k_{AWD} = \frac{J}{(C_s - C_\infty)} \quad (4)$$

where J (mol/cm^2 s) is the average molar flux from the wound bed into the dressing, C_s (mol/cm^3) is the concentration of a solute at the surface of the wound bed, and C_∞ (mol/cm^3) is its concentration in the incoming stream.[27]

In the case of a dissolving substrate such as benzoic acid, we can assume local equilibrium such that the surface concentration is equal to the saturation concentration: $C_s = 2.2 \times 10^{-5}$ mol/cm^3.[28] We measured the mass flow rate by collecting the outlet solution on an analytical balance and the concentration of benzoic acid in the efflux by UV–vis absorbance; from these two values, we obtained the molar flux (mol/s) from the benzoic acid surface for multiple flow rates through the device.

Figure 5 presents plots of the global mass transfer coefficient, k_{AWD}, versus the mass flow rate of liquid through the porous layer, Q (cm^3/s), for three different devices. We fitted these experimental data to a power law function of the form predicted by analysis of the mass transfer in this geometry:

$$k_{AWD} = \frac{J}{(C_s - C_\infty)} = aQ^b \quad (5)$$

For the three devices we measured, we found $0.0010 < a < 0.0022$ and $0.41 < b < 0.55$. We note that there is

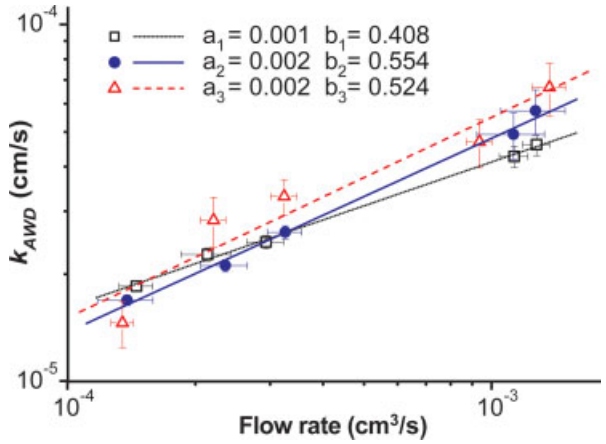

Figure 5. Dependence of the global mass transfer coefficient k_{AWD} (cm/s) on mass flow rate Q (cm^3/s). These data represent three separate AWDs and three benzoic acid substrates. Each symbol (●, □, △) corresponds to a different device and substrate. The AWD was operated on the surface of benzoic acid and the concentration of the acid was measured in the efflux for multiple mass flow rates through the device. Each data point represents three to five separate efflux collections and absorbance readings at a single mass flow rate. Error bars are the propagated uncertainty of absorbance values and mass flow rates. [Color figure can be viewed in the online issue, which is available at www.interscience.wiley.com.]

some degree of variability between the different devices, and within the data points for the device 3. We believe possible sources for this variability to be variations in the structure of the sponge and substrate for different experiments, and channeling of fluid through irregularities in substrate and the pHEMA sponge.

The measured parameters are consistent with predictions of mass transfer into a flow through a porous material, for which b is 0.5;[29] this scaling indicates that the global mass transfer coefficient, k_{AWD}, varies as the square root of the flow rate, Q. The extraction of solute from the wound bed can thus be controlled by varying the externally imposed volumetric flow rate: for example, in order to double the flux of a solute from the surface of a wound, the volume flow rate must be increased by a factor of 4.

To relate the observed rates of mass transfer to the characteristics of the porous exchange layer, we used existing theories of mass transfer within porous media.[29] We can treat the flow through the porous material as a uniform (plug-like) flow of speed v_{eff} (cm/s) over a solid boundary, where v_{eff} is the net speed of fluid along the direction of motion; this speed corresponds to the front velocity of a solution of nonbinding solute (see Figure 4(C) and Elution of Solutes through pHEMA Sponge section). This treatment is valid provided that diffusion within the pores is fast relative to convection, or, stated otherwise, the pore Péclet number, $Pe_{pore} = v_{pore}d_{pore}/D_{BA/water} < 10$. Here, v_{pore} is the fluid velocity in the pore, d_{pore} is the average pore diameter, and $D_{BA/water}$ is the diffusivity of the solute in the fluid. In the case of our wound dressing, the boundary was the wound bed and the porous medium was the pHEMA sponge.

We employed an existing model[29] to express the prefactor, a, in Eq. (5) in terms of the diffusivity of benzoic acid in water, $D_{BA/water}$, the total volume of the device, V, and the tortuosity of the porous medium, τ:

$$a = 1.128\left(\frac{D_{BA/water}}{V}\right)^{0.5}\frac{1}{\tau} \quad (6)$$

Given Eq. (6) and assuming $b = 0.5$, we can predict the mass transfer for a given flow rate through the wound dressing, using the independently obtained tortuosity of the sponge, τ. We estimated the tortuosity of our porous material to be ~ 3 (see Appendix) by using the measured permeability and approximate values for porosity and pore diameter.[21] Using the total volume of the active area of the device ($V = V_m + V_s = 0.625$ cm^3) and the diffusivity of benzoic acid in water[30] ($D_{BA/water} = 8 \times 10^{-6}$ cm^2/s) in Eq. (5), we then predicted that the prefactor for our system should be $a = 0.0013$; this value is consistent with the experimentally observed values ($0.0010 < a < 0.0022$).

Although our results for interfacial mass transfer mediated by the AWD are consistent with the established correlation in Eq. (5), it is useful to point out the conditions for which this correlation might not apply. In our experiments, the Péclet number, Pe_{pore}, ranged from 0.125 to 1.25, indicating that diffusion within the pores was fast relative to convection. If Pe_{pore} were to become large (>10), hydrodynamic dispersion would become important in defining the mass transfer,[31] and at high rates of perfusion or for larger solutes (with low diffusivity), the exponent in Eq. (4) would change to $b = 0.33$. At the maximum mass flow rate (and maximum pore velocity) used for our experiments, the square root scaling may break down for extracted molecules with free diffusivities less than 1×10^{-6} cm^2/s, leading to lower rates of mass transfer relative to the prediction of Eq. (5).

We finish this subsection with two comments regarding the significance of the global coefficient of mass transfer of the AWD as measured on the block of benzoic acid: (1) as mentioned at the start of this section, this measure of the rate of mass transfer is relevant to operation of the AWD on solid substrates that have a much lower Darcy permeabilities than to the pHEMA sponge in the AWD; in this situation, the operation of the AWD leads to negligible convection through the substrate and the mass transfer between the substrate and the AWD occurs by diffusion off of the surface of the substrate into the flow. In the general case of a convectively impermeable substrate, the rate of mass transfer from the tissue will be controlled by the sum of the resistance to transfer through the tissue, ($1/k_{tissue}$) (s/cm), and the resistance to transfer in the AWD, ($1/k_{AWD}$) (s/cm), such that the total coefficient for mass transfer that should be used in calculating flux [via Eq. (4)], k_{total} (cm/s), is given by,

$$\frac{1}{k_{total}} = \frac{1}{k_{AWD}} + \frac{1}{k_{tissue}} \quad (7)$$

Thus, k_{AWD} reported in this section (Figure 5) is an upper bound on mass transfer coefficient provided by the AWD on a solid substrate. (2) As we will discuss in our analysis of the operation of the AWD on a calcium alginate gel in the Operation of AWD section, in the case of a substrate with a non-negligible value of Darcy permeability, the rate of mass transfer achieved with the AWD can be substantially increased, relative to the case of an impermeable substrate, by flow through the substrate.

Operation of AWD

In this section we present results from the operation of the AWD on a slab (1-mm thick) of calcium alginate hydrogel (4 wt % solid). We used this substrate to mimic a soft tissue with a finite Darcy permeability: the calcium alginate hydrogel has a Young's modulus $\sim$170 kPa[32] similar to that of dermal tissue ($\sim$130 kPa),[33] and a Darcy permeability, $\kappa_{alg} = 3 \times 10^{-10}$ cm^2, that lies between that of bone ($\kappa_{bone} \sim 10^{-6}$ cm^2)[34] and other soft tissues (muscle, $\kappa_{muscle} = 2.4 \times 10^{-13}$ cm^2; dermal tissue, $\kappa_{dermis} = 8.7 \times 10^{-14}$ cm^2).[35,36]

Operation of the AWD on a calcium alginate substrate leads to three phenomena: (1) mass transfer from the substrate by diffusive exchange, for a impermeable substrate, as described in the Analysis of Mass Transport through a Porous Material section, (2) mass transfer by convective permeation of the working fluid through the substrate, and (3) mechanical deformation of the substrate. We use this model wound bed to demonstrate both qualitative and quantitative aspects of the operation of the AWD. We finish this section with a discussion of the relevance of these finding for clinical application of the AWD.

Uniform Delivery and Extraction of Solute. The images in Figure 6(A–C) present qualitative demonstration of the use of the AWD for the exchange of small solutes with an alginate wound bed. Figure 6(A) shows a wound bed fully saturated with green food dye; Figure 6(B) shows the same wound bed after application of the AWD for 150 min with a flow of clear buffer (HEPES; flow rate, $Q = 1.0 \times 10^{-3}$ cm^3/s); and Figure 6(C) shows the same model wound bed after application of the AWD for 170 min with a flow of a solution of phenol red (1 m*M* in HEPES buffer; $Q = 1.0 \times 10^{-3}$ cm^3/s). For solutes that do not react with one another (e.g., phenol red and food dye), the processes of delivery and extraction were completely independent and could be carried out simultaneously (data not shown). In a clinical setting, this capability would be useful, for example, for delivery of therapeutic agents with simultaneous assessment of the state of wound through analysis of the exudates; the AWD would allow a clinician to monitor the wound and change the therapeutic regimen as necessary without interrupting the treatment or displacing the wound dressing for collection of exudate.

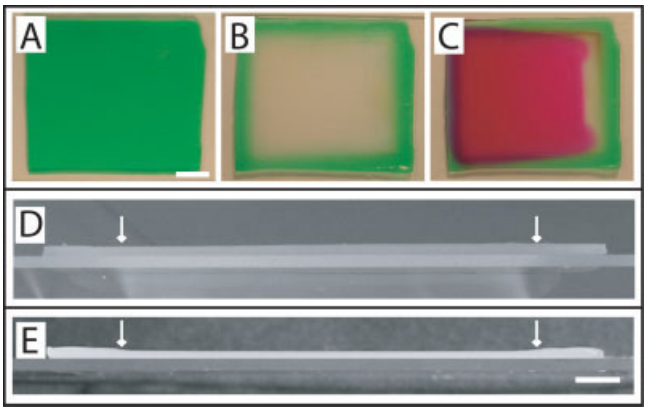

Figure 6. Delivery/extraction experiment. (A–C) Images showing a top view of an alginate gel at various stages of a sequential process of extraction and delivery (scale bar = 1 cm): (A) before extraction (t = 0 min); (B) completed extraction ($t \sim$ 150 min); (C) completed delivery ($t \sim$ 320 min). (D, E) The effect of applied vacuum on the alginate substrate. (D) Alginate gel after application of the AWD for 8 h with low tension ($\sim$14 kPa) in the AWD (flow rate, $Q = 10^{-3}$ cm^3/s); the thickness of the gel remained essentially unchanged (scale bar = 5 mm). (E) Alginate gel after application of the AWD for 120 min at high tension (83 kPa), obtained by using a large resistance upstream of the AWD; the thickness of the gel shows significant compaction. The arrows in (D) and (E) indicate where the edges of the pHEMA sponge where positioned. [Color figure can be viewed in the online issue, which is available at www.interscience.wiley.com.]

Mechanical Deformation of Wound Bed. As stated in the introduction, a potential advantage of the AWD relative to existing active dressings is that it allows mass exchange to be achieved with or without the imposition of significant mechanical stress on the wound bed. To illustrate this point, we operated the dressing under two distinct conditions and observed the deformation induced in the alginate substrate by cutting it with a scalpel in the direction orthogonal to the flow [along y, see Figure 4(C)] immediately after removal of the AWD. Figure 6(D) shows an photograph of the cross-section of a slab of alginate on which the AWD operated for 8 h at a flow rate of 1.0×10^{-3} cm^3/s, as for the experiments in Figure 6(A–C). At this flow rate, the maximum tension experienced by the substrate (as measured that the outlet) was 105 mmHg = 14 kPa. The uniformity of the thickness of the slab indicates that the AWD did not induce significant deformation of the substrate during operation. This result indicates that the AWD can be used to achieve mass exchange [as in Figures 6(A–C)] without imposing significant stress on the wound bed. We note for comparison that the standard stress applied by the VAC is 125 mmHg = 16.7 kPa. Figure 6(E) shows a cross-section of a slab of alginate on which the AWD operated for 120 min at a maximum tension of 600 mmHg = 83 kPa, obtained by placing a large resistance upstream of the AWD. As is apparent in the photograph, this level of tension resulted in considerable compression ($\sim$40% reduction in thickness) of the alginate in the region exposed to the pHEMA sponge of the substrate. While this level of

vacuum is not recommended clinically,[37] this result indicates that the AWD can be used to stimulate the wound bed mechanically as well as chemically.

Analysis of Solutes in Exudate. We turn to the analysis of the temporal evolution of the concentration of solutes in the efflux of the AWD as it is operated on either solid (benzoic acid) or soft (calcium alginate) substrates. These experiments allow us to demonstrate the operation of the AWD with both small and large solute and to gain insight into the transient chemical signal that can be observed at the outlet of the AWD for diagnostic applications. Figure 7 presents the temporal evolution of the concentration of solute in fractions of the fluid exiting the wound dressing in the initial period after beginning operation on a block of benzoic acid, on an alginate gel initially saturated with a solution of fluorescein (initial concentration, $C_0 = 100\ \mu M$ in buffer), or on an alginate gel initially saturated with fluorescently labeled bovine serum albumin (initial concentration, $C_0 = 50\ \mu M$ in buffer).

In all three cases presented in Figure 7, the concentration observed at the outlet of the AWD rises initially. In the case of benzoic acid, this rise terminates in a plateau concentration. This steady state concentration is maintained because the dissolution of the solid maintains a constant concentration the bottom surface of the AWD. This steady state value was used to determine the coefficients of mass transfer, k_{AWD}, presented in Figure 5. In contrast, when the AWD was operated on alginate, the concentration passed through a maximum before dropping to zero. This failure to reach a plateau value was due to the depletion of the solute from the substrate. With this depletion, the transfer of out of the substrate eventually became the rate limiting step in the exchange process [i.e., $k_{tissue} > k_{AWD}$ in Eq. (7)]. Eventually, the substrate also became entirely emptied of the solute, as shown graphically in Figure 6(B). We note that benzoic acid and FITC-BSA were evacuated more rapidly than fluorescein. The slower rate of elution of fluorescein was due to the affinity of this solute for the pHEMA sponge (see Table I). In each case, the time required to reach the plateau or maximum corresponded closely to the retention time, t_r [Eq. (3)].

Finally, we note that the complete extraction of FITC-BSA occurred within an interval of time ($\sim$150 min) that was too short to be explained by purely diffusive mass transfer within the alginate substrate. A simple prediction for the time for FITC-BSA to diffuse across a 1 mm-thick gel is, $t_{diff} \sim (\text{thickness})^2/2D_{BSA/gel} \sim 5 \times 10^4$ s $\sim$800 min. This observation suggests that the AWD was driving flow through the substrate such that solute was convected to the outlet without diffusing to the interface with the AWD; this mechanism is likely to become important relative to diffusion for large solutes at long times. The permeation of the alginate is not unreasonable given that the Darcy permeability of the gel is nonnegligible relative to that of the pHEMA sponge: $\kappa_{alg}/\kappa_{pHEMA} = 0.15$.

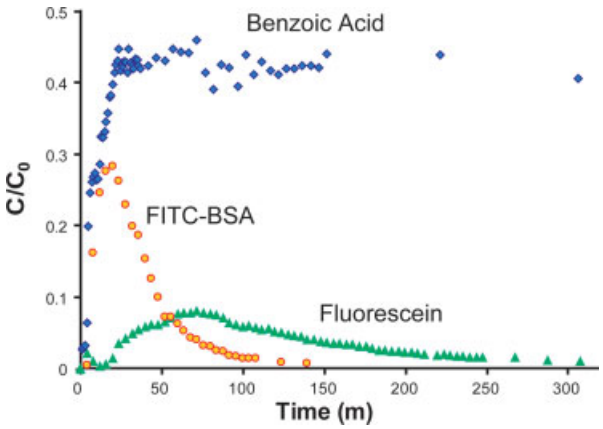

Figure 7. Time dependence of concentration of solute observed in exudates. The fluid exiting the AWD was collected to quantify the amount of solutes extracted as a function of time. Diamonds correspond to the benzoic acid, the circles correspond to a FITC-BSA, and triangles correspond to fluorescein. The concentrations are all normalized by initial solute concentration: 22 μM for benzoic acid (this value is the saturation concentration that is maintained at the surface of the dissolving solid = C_s), 50 μM for FITC-BSA, and 100 μM for fluorescein). The following experimental conditions applied to all experiments: flow rate = 1.1×10^{-3} cm^3/s; composition of substrate = benzoic acid disc or calcium alginate gels; thickness of alginate gel substrates = 1 mm. [Color figure can be viewed in the online issue, which is available at www.interscience.wiley.com.]

These results give us guidance regarding the performance of the AWD in potential clinical applications. Of particular interest is the implication for binding solutes: if the AWD is used to wash a particular solute out of a wound bed, one can expect significant retardation of the extraction process for solutes with affinity for the pHEMA. A possible route to circumventing binding could be a surface modification of the pHEMA; such an approach would require the use of passivating molecules such as poly(ethylene glycol) that would not have deleterious effects on the wound bed.

Mass Exchange Within Multiple Regions Within the Wound Bed. A desirable feature in an advanced wound dressing would be the ability to exchange solute selectively with different regions of a wound. By creating impermeable barriers within the pHEMA layer, we confined the flow pattern inside the pHEMA sponge to three separate regions (Formation of Preparation of Porous pHEMA Hydrogel section), each with independent reservoirs and fluidic connections. By using distinct fluids for each inlet reservoir, it was possible to flow three separate streams inside the sponge, and transfer the resulting pattern onto the substrate.

Figure 8 illustrates this mode of operation with a solution of phenol red, a clear buffer, and a solution of green dye as the separate incoming fluids. A comparison of the dye patterns in the pHEMA sponge (frame (A)) and in the substrate (frame (B)) confirmed the fidelity of the transfer process.

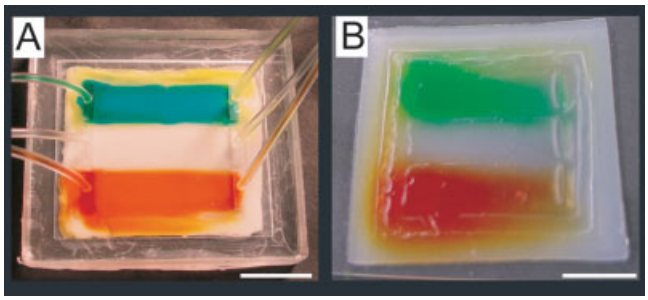

Figure 8. Patterned delivery of solutes. (A) Top view of AWD acting on a calcium alginate substrate after operation for 120 min to deliver three separate solutes. (B) Top view of corresponding patterned substrate. The scale bars in both images correspond to 1 cm. [Color figure can be viewed in the online issue, which is available at www.interscience.wiley.com.]

The ability to control infusion over independent regions of a wound would be useful, for example (1) when delivering gradients of solutes to direct cell migration as part of the re-epithelialization process, or (2) when collection of exudate from different regions of the wound would help assess the progress of the healing process. In either case, the spatial resolution of the distinct zones would be limited by the separation between the barriers, and the minimum barrier width that can retain structural integrity. Based on observation of shape and strength of the polymerized barriers, we expect to obtain submillimeter minimum feature sizes with the method described in the Preparation of Porous pHEMA Hydrogel section. The introduction of solid barriers also makes it possible to maintain each region at different negative pressures, making it possible to turn off flow in some of the regions, or infuse/extract from each region at different rates.

CONCLUSION

We described material characterization, device fabrication and basic operation of an AWD. This AWD allowed for mass exchange with a substrate with both spatial and temporal control. The delivery of solutes demonstrated the feasibility of using this device to act as a therapeutic tool; the collection of solutes indicated the possible use in "diagnostic mode" for continuous assessment of wounds. Furthermore, the methods of characterization of mass transfer shown here may be useful as tools to elucidate the different modes of action of other AWDs, such as the VAC®. In particular, we believe it would be valuable to distinguish the role of convective mass transfer from that of mechanical stress.

We have also identified potential limitations that may need to be addressed for the implementation of our AWD in the clinic. Some of these limitations stem from the differences between the properties of real wound beds and the models used in this study. For instance, exudative wounds will produce fluid and add convective mass transfer to the diffusive mass transfer studied here: using data from James et al.[4] we estimate that the AWD would have to evacuate an additional 0.5×10^{-3} cm^3/min/cm^2, corresponding to $\sim 3 \times 10^{-3}$ cm^3/min in a device such as the one described here; this extra flow is well within the operating range of the AWD.

The implementation of the AWD on arbitrary wound shapes poses another potential challenge, in that it would be impossible to fabricate AWDs to fit every possible wound shape. A possible approach would be to use a device with an active area that is larger than the footprint of the wound bed, and apply an inert sealant (i.e., vaseline) to the edge of the wound; the sealant would occlude the area of the device outside the wound site, ensuring that healthy tissue around it is not affected by the AWD. For larger wounds, a combination of devices running in parallel could be used; our demonstration of operation with barriers supports the hypothesis that independent regions from distinct devices could be operated side by side without interfering with one another.

We would like to thank Dr. Roger Yurt and Dr. Lisa Staiano-Coico (Cornell Weill Medical College), and Dr. Deepak Kilpadi (Kinetic Concepts), for insightful discussions; David Putnam for use of his spectrometer and fluorescence reader; Glenn Swan for technical assistance.

REFERENCES

1. Monafo WW. Current concepts—Initial management of burns. N Engl J Med 1996;335:1581–1586.
2. Martin P. Wound healing—Aiming for perfect skin regeneration. Science 1997;276:75–81.
3. Singer AJ, Clark RAF. Mechanisms of disease—Cutaneous wound healing. N Engl J Med 1999;341:738–746.
4. James TJ, Hughes MA, Cherry GW, Taylor RP. Simple biochemical markers to assess chronic wounds. Wound Repair Regen 2000;8:264–269.
5. Goova MT, Li J, Kislinger T, Qu W, Lu Y, Bucciarelli LG, Nowygrod S, Wolf BM, Caliste X, Yan SF, Stern DM, Schmidt AM. Blockade of receptor for advanced glycation end-products restores effective wound healing in diabetic mice. Am J Pathol 2001;159:513–525.
6. Burke JF, Yannas IV, Quinby WC, Bondoc CC, Jung WK. Successful use of a physiologically acceptable artificial skin in the treatment of extensive burn injury. Ann Surg 1981;194:413–428.
7. Yannas IV, Burke JF, Warpehoski M, Stasikelis P, Skrabut EM, Orgill DP, Giard D. Design principles and preliminary clinical-performance of an artificial skin. In: Cooper SL, Peppas NA, editors. Biomaterials: Interfacial Phenomena and Applications. Advances in Chemistry Series No. 199. Washington, DC: American Chemistry Society; 1982. p. 475–481.
8. Chan ESY, Lam PK, Liew CT, Lau HCH, Yen RSC, King WWK. A new technique to resurface wounds with composite biocompatible epidermal graft and artificial skin. J Trauma Inj Infect Crit Care 2001;50:358–362.
9. Griffiths M, Livingstone R, Price R, Navsaria H. Survival of apligraf in acute human wounds. Tissue Eng 2004;10:1180–1195.
10. Shirakata Y, Tokumaru S, Yamasaki K, Sayama K, Hashimoto K. So-called biological dressing effects of cultured epidermal sheets are mediated by the production of EGF family, TGF-β and VEGF. J Dermatol Sci 2003;32:209–215.

11. Morykwas MJ, Argenta LC. Use of negative-pressure to increase the rate of granulation-tissue formation in chronic open wounds. FASEB J 1993;7:A138–A138.
12. Morykwas MJ, Argenta LC, SheltonBrown EI, McGuirt W. Vacuum-assisted closure: A new method for wound control and treatment. Animal studies and basic foundation. Ann Plast Surg 1997;38:553–562.
13. Webb LX. New techniques in wound management: Vacuum-assisted wound closure. J Am Acad Orthop Surg 2002;10:303–311.
14. Eginton MT, Brown KR, Seabrook GR, Towne JB, Cambria RA. A prospective randomized evaluation of negative-pressure wound dressings for diabetic foot wounds. Ann Vasc Surg 2003; 17:645–649.
15. Lambert KV, Hayes P, McCarthy M. Vacuum assisted closure: A review of development and current applications. Eur J Vasc Endovasc Surg 2005;29:219–226.
16. Saxena V, Hwang CW, Huang S, Eichbaum Q, Ingber D, Orgill DP. Vacuum-assisted closure: Microdeformations of wounds and cell proliferation. Plastic Reconstr Surg 2004;114:1086–1096.
17. Liu Q, Hedberg EL, Liu ZW, Bahulekar R, Meszlenyi RK, Mikos AG. Preparation of macroporous poly(2-hydroxyethyl methacrylate) hydrogels by enhanced phase separation. Biomaterials 2000;21:2163–2169.
18. McDonald JC, Chabinyc ML, Metallo SJ, Anderson JR, Stroock AD, Whitesides GM. Prototyping of microfluidic devices in poly(dimethylsiloxane) using solid-object printing. Anal Chem 2002;74:1537–1545.
19. Revzin A, Russell RJ, Yadavalli VK, Koh WG, Deister C, Hile DD, Mellott MB, Pishko MV. Fabrication of poly(ethylene glycol) hydrogel microstructures using photolithography. Langmuir 2001;17:5440–5447.
20. Chang SCN, Rowley JA, Tobias G, Genes NG, Roy AK, Mooney DJ, Vacanti CA, Bonassar LJ. Injection molding of chondrocyte/alginate constructs in the shape of facial implants. J Biomed Mater Res 2001;55:503–511.
21. Scheidegger AE. The Physics of Flow Through Porous Media. Toronto: University of Toronto Press; 1960.
22. Perry RH, Green DW. Chemical Engineers' Handbook. New York: McGraw-Hill; 1997.
23. Strop P, Mikes F, Chytilova Z. Hydrophobic interaction chromatography of proteins and peptides on spheron P-300. J Chromatogr 1978;156:239–254.
24. Ravindranath B. Principles and practice of chromatography. Chichester: Ellis Horwood; 1989.
25. Weiss JA, Maakestad BJ. Permeability of human medial collateral ligament in compression transverse to the collagen fiber direction. J Biomech 2006;39:276–283.
26. Gu WY, Yao H, Huang CY, Cheung HS. New insight into deformation-dependent hydraulic permeability of gels and cartilage, and dynamic behavior of agarose gels in confined compression. J Biomech 2003;36:593–598.
27. Bird RB, Stewart WE, Lightfoot EN. Transport Phenomena. New York: John Wiley and Sons; 1960.
28. CRC Handbook of Chemistry and Physics. CRC Press: Boca Raton, FL; 1996.
29. Bejan A. Convection Heat Transfer. New York: John Wiley and Sons; 1995.
30. Irandoust S, Andersson B. Concentration-dependent diffusivity of benzoic-acid in water and its influence on the liquid solid mass-transfer. Can J Chem Eng 1986;64:954–959.
31. Koch DL. Hydrodynamic diffusion near solid boundaries with applications to heat and mass transport into sheared suspensions and fixed-fibre beds. J Fluid Mech 1996;318:31–47.
32. Stevens MM, Qanadilo HF, Langer R, Shastri VP. A rapid-curing alginate gel system: Utility in periosteum-derived cartilage tissue engineering. Biomaterials 2004;25:887–894.
33. Diridollou S, Patat F, Gens F, Vaillant L, Black D, Lagarde JM, Gall Y, Berson M. In vivo model of the mechanical properties of the human skin under suction. Skin Res Technol 2000;6:214–221.
34. Kohles SS, Roberts JB, Upton ML, Wilson CG, Bonassar LJ, Schlichting AL. Direct perfusion measurements of cancellous bone anisotropic permeability. J Biomech 2001;34:1197–1202.
35. Zakaria ER, Lofthouse J, Flessner MF. In vivo hydraulic conductivity of muscle: Effects of hydrostatic pressure. Am J Physiol Heart Circ Physiol 1997;42:H2774–H2782.
36. Levick JR. Flow through interstitium and other fibrous matrices. Q J Exp Physiol Cogn Med Sci 1987;72:409–438.
37. Morykwas MJ, Faler BJ, Pearce DJ, Argenta LC. Effects of varying levels of subatmospheric pressure on the rate of granulation tissue formation in experimental wounds in swine. Ann Plastic Surg 2001;47:547–551.
38. Bennett D, Burford RP, Davis TP, Tilley HJ. Synthesis of porous hydrogel structures by polymerizing the continuous phase of a microemulsion. Polym Int 1995;36:219–226.

APPENDIX

Theory of Flow in Porous Media

We follow Bejan's treatment of mass transfer based upon a uniform Darcy flow through a homogeneous and isotropic porous medium at low Peclet number. Under these assumptions, the global Sherwood number (*Sh*—a nondimensional mass transfer coefficient) is related to the Peclet number (*Pe*) as in the expression below:

$$Sh = 1.128Pe^{0.5} \tag{A1}$$

where

$$Sh = \frac{k_{\text{total}}L_{\text{eff}}}{D_{\text{eff}}}, \tag{A2}$$

$$Pe = \frac{v_{\text{eff}}L_{\text{eff}}}{D_{\text{eff}}}, \tag{A3}$$

D_{eff} (cm^2/s) is the solute diffusivity in the porous medium, L_{eff} (cm) is the effective flow path length, v_{eff} (cm/s) is the dye front velocity, and k_{AWD} (cm/s) is the global mass transfer coefficient for nondissolving substrates.

We are interested in relating the mass transfer coefficient, k_{AWD}, to the observed macroscopic quantities (such as Q), but Eqs. (A1)–(A3) depend upon the microscopic structure of the porous material. For example, a fluid particle must travel an effective flow path of length L_{eff}, which is larger than the macroscopic length of the porous medium length, L. The ratio of the length of true flow path to the macroscopic length of the system in the direction of macroscopic flux is the tortuosity of the material, $\tau = L_{\text{eff}}/L$.[21] In addition, the actual velocity of a fluid particle within a porous medium (v_{eff}) is larger than the volume flow rate (Q) divided by the macroscopic cross-sectional area (A) of the device due to the reduced area available for flow, A_{eff}. We were able to directly measure v_{eff} by following a front of dye (nonbinding) as it moved across the device. With this measurement and the known volume flow rate, we extracted the effective area ($A_{\text{eff}} = Q/v_{\text{eff}}$). Also, the diffusive transport of a solute within a porous medium (D_{eff}) is

decreased relative to the diffusivity of the solute in free solution ($D_{BA/water}$) due to porous nature of the medium. This effective diffusivity must also be taken into account when comparing experiment to theory. In light of these microscopic properties which affect flow through a porous medium, we define the following quantities:

$$\tau = \frac{L_{eff}}{L} \tag{A4}$$

$$D_{eff} = \left(\frac{A_{eff}}{A}\right)\frac{1}{\tau}\, D_{BA/water} \tag{A5}$$

$$A_{eff} = \frac{Q}{v_{eff}} \tag{A6}$$

We can thus rewrite Eq. (A1) as

$$k_{AWD} = 1.128\left(\frac{D_{BA/water}}{\tau}\,\frac{A_{eff}}{A}\,\frac{1}{\tau L}\,\frac{1}{A_{eff}}\right)^{0.5} Q^{0.5} = 1.128\left(\frac{D_{BA/water}}{AL\tau^2}\right)^{0.5} Q^{0.5} \tag{A7}$$

We obtain the tortuosity, τ, by deriving Darcy's Law within the capillary theory by Kozeny,[21] and expressing the permeability of the material, κ_{pHEMA}, as:

$$k_{pHEMA} = \frac{\varphi d_{pore}^2}{32\tau^2} \tag{A8}$$

Here, φ is the porosity of the medium (void fraction of total volume), τ is its tortuosity, κ_{pHEMA} is the permeability (cm^2) measured by the drip experiment (see Measurement of Hydraulic Permeability of pHEMA Sponge and Calcium Alginate Gel section), and d is the average pore size (cm) estimated from SEM images (such as those in Figure 3).

Expressing Eq. (A6) in this way has the advantage of presenting our results in terms of measurable and known quantities. The permeability was measured using the water column drip experiment ($\kappa_{pHEMA} = 2.0 \times 10^{-9}$ cm^2), and the pore size was estimated from SEM images ($d_{pore} \sim 10$ μm). Finally, the porosity of our pHEMA sponge was estimated in two ways: (1) the effective area for flow (A_{eff}) divided by the total area (A) gives an estimate of V_s/V ($\varphi \sim 0.52$), and (2) use of the known volume fraction of HEMA and water in the initial prepolymer solution in combination with the literature values for the equilibrium water content of pHEMA also gives an estimate of the porosity ($\varphi \sim 0.53$).[38] We used these values of φ, d_{pore}, and κ_{pHEMA} to obtain a value of $\tau \sim 3$ based on Eq. (A7). We then used this value of τ from Eq. (A6) in Eq. (6).